International Journal of
MATERIALS RESEARCH

Zeitschrift für METALLKUNDE

Original Contributions

Jiangtao Gao, Changrong Li, Cuiping Guo, Zhenmin Du
School of Materials Science and Engineering, University of Science and Technology Beijing, Beijing, P.R. China

Solidification processes of as-cast alloys and phase equilibria at 1 300 °C of the Nb–Si–V ternary system

The liquidus projection and the isothermal section at 1 300 °C of the Nb–Si–V ternary system were experimentally studied. Using scanning electron microscopy, electron probe microanalysis and X-ray diffraction, the primary solidification phases and the precipitation paths in each region of the liquidus projection as well as the equilibrium relations of the phases in the isothermal section were determined. Ten primary solidification regions were found in the liquidus projection and eight three-phase equilibrium regions were observed in the isothermal section at 1 300 °C. The compounds βNb_5Si_3 with V_5Si_3 and $NbSi_2$ with VSi_2 are the phases of the same structure but different compositions and form two linear compounds $\beta Nb(V)_5Si_3$ or $V(Nb)_5Si_3$ and $Nb(V)Si_2$ or $V(Nb)Si_2$, respectively The ternary linear compound $(Nb,V)_2Si$ with the stoichiometry about 2 : 1 of (Nb + V) : Si was found in both the liquidus projection and the isothermal section at 1 300 °C.

Keywords: Nb–Si–V ternary system; Liquidus projection; Isothermal section 1 300 °C

1. Introduction

In the multi-component Nb–Si-based alloy systems, the balance of the mechanical properties such as room temperature toughness, high temperature creep resistance and oxidation resistance can be achieved by adding alloying elements to stabilize intermetallic compounds and by forming Laves phase to improve the oxidation resistance [1–3]. The addition of V can promote the transformation of $Nb_3Si \rightarrow$ bcc + Nb_5Si_3, increase the volume fraction of Nbss/Nb_5Si_3 in-situ composites. The bcc solid solution phase Nbss provides room temperature toughness and ductility, and the Nb_5Si_3 intermetallic compound provides high temperature strength. Nbss/Nb_5Si_3 in-situ composites exhibit well-balanced mechanical propertie [4, 5]. Kim et al. [6] found that V not only reduced the stability of Nb_3Si and promoted its decomposition, but also directly formed the phase of αNb_5Si_3. At the same time, due to the solid solution strengthening effect and the elastic interaction caused by the size difference between Nb and V atoms, adding V to Nb–Si-based compounds can improve the room temperature strength of the alloy [7, 8]. In summary, V is an important alloying element in optimizing the properties of the Nb–Si based superalloys [9]. Therefore, the study of the phase equilibria of the Nb–Si–V ternary system is of great practical significance. Geng et al. [10] made a comprehensive evaluation of the experimental phase equilibria, crystal structures and thermochemical properties and therefore assessed the Gibbs free energies of all the phases of the system. The Nb–Si binary system includes the solid solution phases bcc(Nb) and Diamond(Si), the intermetallic compounds Nb_3Si, αNb_5Si_3, βNb_5Si_3, $NbSi_2$ and the liquid phase. The V–Si binary system was optimized by Zhang et al. [11]. The V–Si binary system includes the solid solution phases bcc(V) and Diamond(Si), four stable intermetallic compounds V_3Si, V_5Si_3, V_6Si_5 [12], VSi_2, and the liquid phase. Kumar et al. [13] considered that Nb and V are infinitely soluble with each other in both of the liquid and the solid phases of the Nb–V

binary system, The present authors, Gao et al. [14] observed the existence of a miscibility gap and spinodal decomposition in the low temperature region ($T < 804$ °C), and re-optimized the system accordingly. There are few early reports of the phase equilibria of the Nb–Si–V ternary system [15, 16]. Li et al. [17] measured the phase equilibrium relations of the Nb–Si–V ternary system at three temperatures of 1 100, 1 200 and 1 300 °C and found a new linear-stoichiometric compound $(Nb,V)_2Si$, There are relatively few studies on the liquidus projection of the system. The isothermal section of the Nb–Si–V ternary system at

1 300 °C determined by Li et al. [17] and binary phase diagrams [10, 11, 14] constituting the ternary system are shown in Fig. 1.

In order to assess the Nb–Si–V ternary system thermodynamically, the experimental liquidus projection is essential for determining the phase relations between the liquid phase and the primary solidified phase as well as for analyzing the solidification paths of the as-cast alloys. In addition, the newly found linear stoichiometric compound $(Nb,V)_2Si$ needs to be further confirmed. Therefore, the present study targets the solidification processes of the as-cast alloys and the phase equilibria at 1 300 °C of the Nb–Si–V ternary system.

2. Experimental procedure

Niobium (99.95 wt.%), silicon (99.99 wt.%) and vanadium (99.99 wt.%) from Trillion Metals Co. Ltd. were used as the raw materials, and then were melted into 5 g button-like specimens by vacuum arc furnace. Each alloy specimen was turned over at least 3 times during the melting process to ensure a sufficiently homogeneous composition. In the meanwhile, some sponge titanium was used to absorb oxygen. The weight losses of the prepared alloys were less than 1 %. The as-cast alloys were ground and then polished directly to study the liquidus projection. Specimens sealed

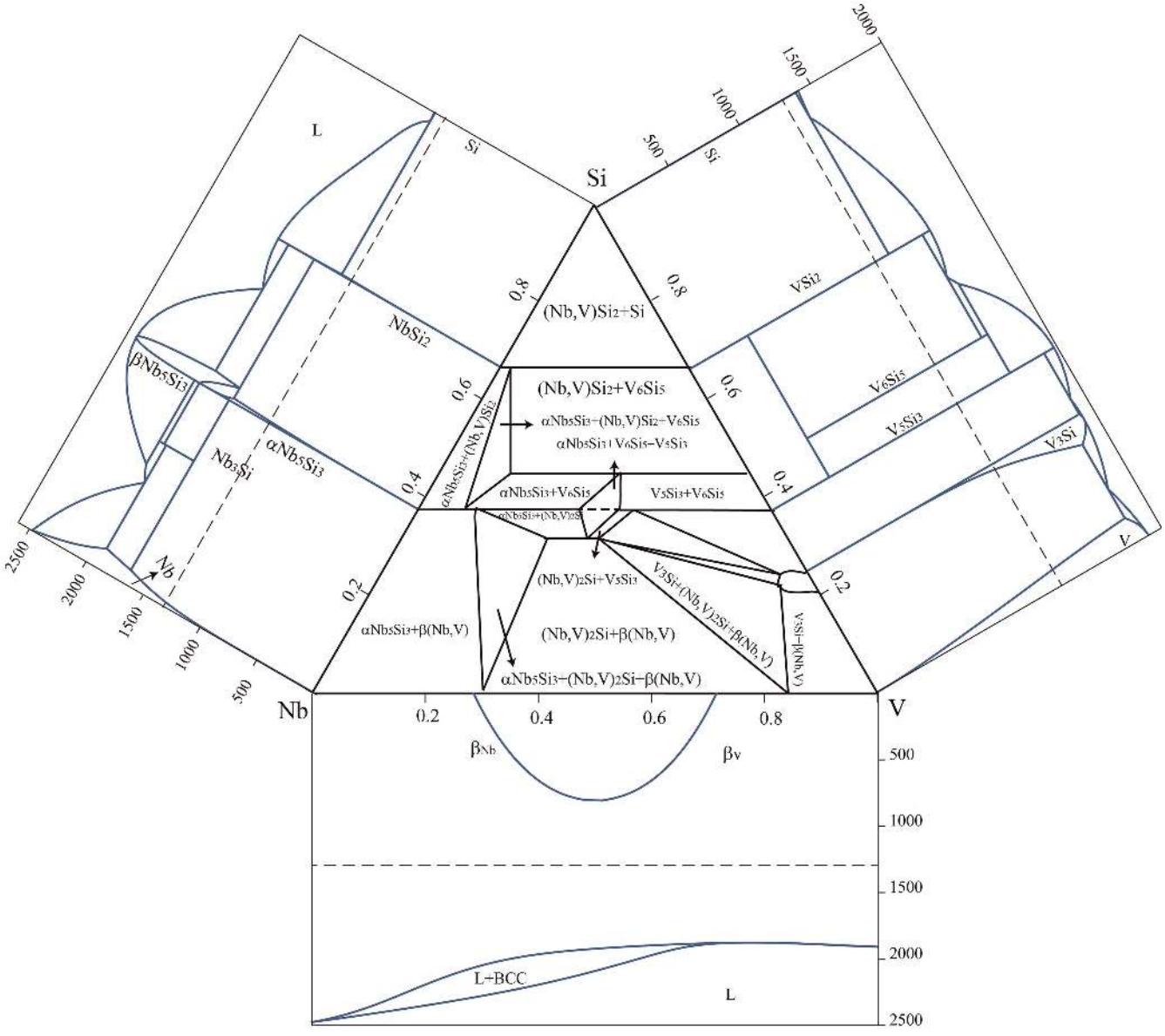

Fig. 1. Binary phase diagrams constituting the Nb–Si–V ternary system [10, 11, 14] and the isothermal section at 1 300 °C determined by Li et al. [17].

in argon filled quartz tubes were isothermally treated at 1 300 °C for 240 h, and were then used to study the isothermal section. The microstructural observation, the phase identification and the composition determination were performed by using SEM (scanning electron microscopy, JSM-6480LV), XRD (X-ray diffraction, STOFDARMSTADT-STOE/2, 3 KW) and EPMA (electron probe microanalysis, GEOLJXA-8230), respectively.

3. Results and discussion

3.1. Experimental results of the liquidus projection

The information of all the stable binary solid phases in the Nb–Si, the V–Si and the Nb–V binary systems constituting the Nb–Si–V ternary system is summarized in Table 1 [18–20]. From Table 1, it can be seen that βNb_5Si_3 and V_5Si_3, just like $NbSi_2$ and VSi_2, are phases of the same structure but different compositions, while Nb_3Si and V_3Si are the phases of the same stoichiometry but different structures. Therefore, in the Nb–Si–V ternary system, βNb_5Si_3 with V_5Si_3 and $NbSi_2$ with VSi_2 form two linear compounds, $\beta Nb(V)_5Si_3$ or $V(Nb)_5Si_3$ and $Nb(V)Si_2$ or $V(Nb)Si_2$.

In the present work, a series of as-cast alloys have been studied. The primary solidification phases, the compositions of the constituent phases and the precipitation paths of the alloys are listed in Table 2. There is no report on the structural refinement of the newly observed linear-stoichiometric compound $(Nb,V)_2Si$. The constructed liquidus projection for the Nb–Si–V ternary system is shown in Fig. 2.

In general, the phase with the largest morphology or the dendritic structure in the SEM/BSE image is the primary phase precipitated directly from the liquid, which is determined by combining XRD analysis and EPMA determination. The secondary solidified phase and the related reaction type are determined according to the morphology next to the primary phase. If a phase adjoining the primary phase is formed, a peritectic reaction is occurring concurrently, (primary phase) + liquid → (secondary phase). Here after, the secondary phase precipitates directly from the liquid. While if a microstructure with the two-phase eutectic feature, usually with a finer microstructure than that of the primary phase, is formed near the primary phase, a eutectic reaction occurs, liquid → (primary phase) + (secondary phase). Sometimes, the peritectic reactions occur successively, one after another. Occasionally, a three-phase eutectic microstructure is formed with the finest morphology after the two-phase eutectic. In such a way, the solidification process continues until the liquid phase is exhausted. Typical SEM/BSE micrographs and the X-ray diffractograms are analyzed as follows.

3.1.1. The primary phase of $Nb(V)Si_2$

SEM/BSE images of the as-cast alloys of A1# Nb-70Si-10V and A2# Nb-70Si-20V are shown in Fig. 3a and b, respectively. Combined with the results of XRD patterns Fig. 3c, the microstructures of A1# and A2# samples are composed of the primary phase $Nb(V)Si_2$, (the bright white phase) and the subsequently solidified phases $V(Nb)Si_2$ (the

Table 1. The stable solid phases in the Nb–Si, the Nb–V and the Si–V binary systems.

System	Phase	Pearson's symbol	Prototype	Strukturbericht designation	References
Nb–Si	bcc(Nb)	cI2	W	A2	[18]
	Nb_3Si	tP32	PTi_3	…	[18]
	βNb_5Si_3	tI32	Si_3W_5	$D8_m$	[18]
	αNb_5Si_3	tI32	Cr_5B_3	$D8_l$	[18]
	$NbSi_2$	hP9	$CrSi_2$	C40	[18]
	Diamond(Si)	cF8	C(Diamond)	A4	[18]
Nb–V	bcc(Nb)	cI2	W	A2	[19]
	bcc(V)	cI2	W	A2	[19]
V–Si	Diamond(Si)	cF8	C(Diamond)	A4	[20]
	V_3Si	cP8	Cr_3Si	A15	[20]
	V_5Si_3	tI32	Si_3W_5	D8m	[20]
	V_6Si_5	oI44	Nb_6Sn_5	…	[20]
	VSi_2	hP9	$CrSi_2$	C40	[20]
	bcc(V)	cI2	W	A2	[20]

Table 2. Constituent phases and solidification paths of the Nb–Si–V as-cast alloys.

Primary phase	Nominal composition (at.%)	As-cast phases	Phase composition (at.%)			Precipitation paths
			Nb	Si	V	
$Nb(V)Si_2$	Nb-70Si-10V(A1#)	$Nb(V)Si_2$ $V(Nb)Si_2$ Diamond(Si)	27.27	67.54	5.18	$L \rightarrow Nb(V)Si_2$
			14.94	66.98	18.08	$L + Nb(V)Si_2 \rightarrow V(Nb)Si_2$
			0	99.13	0.07	$L \rightarrow Nb(V)Si_2 + V(Nb)Si_2$+ Diamond(Si)
	Nb-70Si-20V(A2#)	$Nb(V)Si_2$	18.97	67.95	13.08	$L \rightarrow Nb(V)Si_2$
		$V(Nb)Si_2$	6.66	65.58	27.76	$L + Nb(V)Si_2 \rightarrow V(Nb)Si_2$
		Diamond(Si)	0.17	99.46	0.37	$L \rightarrow Nb(V)Si_2 + V(Nb)Si_2$ + Diamond(Si)
$V(Nb)Si_2$	Nb-60Si-39V(A3#)	$V(Nb)Si_2$	0.21	68.5	31.29	$L \rightarrow V(Nb)Si_2$
		$V(Nb)_6Si_5$	0.67	46.59	52.74	$L \rightarrow V(Nb)_6Si_5 + V(Nb)Si_2$
$V(Nb)_5Si_3$	Nb-55Si-42V(A4#)	$V(Nb)_5Si_3$	5.74	37.51	56.75	$L \rightarrow V(Nb)_5Si_3$
		$V(Nb)Si_2$	2.53	66.54	30.93	$L \rightarrow V(Nb)Si_2 + V(Nb)_5Si_3$
	Nb-40Si-57V(A5#)	$V(Nb)_5Si_3$	5.93	36.61	57.46	$L \rightarrow V(Nb)_5Si_3$
		$V(Nb)Si_2$	1.97	65.3	32.73	$L \rightarrow V(Nb)Si_2 + V(Nb)_5Si_3$
	Nb-55Si-30V(A6#)	$V(Nb)_5Si_3$	3.65	35.52	59.82	$L \rightarrow V(Nb)_5Si_3$
		$Nb(V)Si_2$	21.26	66.01	12.73	$L \rightarrow V(Nb)_5Si_3 + Nb(V)Si_2$
		$V(Nb)Si_2$	5.63	67.49	26.88	$L + Nb(V)Si_2 \rightarrow V(Nb)_5Si_3 + V(Nb)Si_2$
	Nb-50Si-40V(A7#)	$V(Nb)_5Si_3$	16.62	36.49	46.89	$L \rightarrow V(Nb)_5Si_3$
		$Nb(V)Si_2$	17.06	67.43	15.51	$L \rightarrow V(Nb)_5Si_3 + Nb(V)Si_2$
		$V(Nb)Si_2$	3.36	67.55	29.09	$L + Nb(V)Si_2 \rightarrow V(Nb)_5Si_3 + V(Nb)Si_2$
	Nb-50Si-35V(A8#)	$V(Nb)_5Si_3$	22.46	36.5	41.05	$L \rightarrow V(Nb)_5Si_3$
		$Nb(V)Si_2$	21.08	66.7	12.22	$L \rightarrow V(Nb)_5Si_3 + Nb(V)Si_2$
		$V(Nb)Si_2$	2.15	66.95	30.9	$L + Nb(V)Si_2 \rightarrow V(Nb)_5Si_3 + V(Nb)Si_2$
	Nb-40Si-40V(A9#)	$V(Nb)_5Si_3$	23.54	36.85	39.62	$L \rightarrow V(Nb)_5Si_3$
		$\beta Nb(V)_5Si_3$	33.57	36.35	30.08	$L \rightarrow V(Nb)_5Si_3 + \beta Nb(V)_5Si_3$
		$V(Nb)_3Si$	10.34	27.56	62.11	$L \rightarrow V(Nb)_5Si_3 + \beta Nb(V)_5Si_3 + V(Nb)_3Si$
	Nb-30Si-60V(A10#)	$V(Nb)_5Si_3$	13.32	37.83	48.85	$L \rightarrow V(Nb)_5Si_3$
		$V(Nb)_3Si$	3.01	26.59	70.40	$L \rightarrow V(Nb)_5Si_3 + V(Nb)_3Si$
		$\beta Nb(V)_5Si_3$	25.06	36.35	39.56	$L \rightarrow \beta Nb(V)_5Si_3 + V(Nb)_5Si_3 + V(Nb)_3Si$
	Nb-30Si-50V(A11#)	$V(Nb)_5Si_3$	20.52	37.83	41.65	$L \rightarrow V(Nb)_5Si_3$
		$V(Nb)_3Si$	5.32	26.04	68.64	$L \rightarrow V(Nb)_5Si_3 + V(Nb)_3Si$
		$\beta Nb(V)_5Si_3$	33.15	36.35	30.5	$L \rightarrow \beta Nb(V)_5Si_3 + V(Nb)_5Si_3 + V(Nb)_3Si$

Primary phase	Nominal composition (at.%)	As-cast phases	Phase composition (at.%)			Precipitation paths
			Nb	Si	V	
$\beta Nb(V)_5Si_3$	Nb-50Si-15V(A12#)	$\beta Nb(V)_5Si_3$	48.14	37.33	14.53	$L \rightarrow \beta Nb(V)_5Si_3$
		$Nb(V)Si_2$	27.91	68.88	3.21	$L \rightarrow \beta Nb(V)_5Si_3 + Nb(V)Si_2$
		$V(Nb)_5Si_3$	28.19	36.72	35.09	$L + \beta Nb(V)_5Si_3 \rightarrow Nb(V)Si_2 + V(Nb)_5Si_3$
	Nb-50Si-22V(A13#)	$\beta Nb(V)_5Si_3$	39.16	37.08	23.76	$L \rightarrow \beta Nb(V)_5Si_3$
		$Nb(V)Si_2$	24.04	65.85	10.11	$L \rightarrow \beta Nb(V)_5Si_3 + Nb(V)Si_2$
		$V(Nb)_5Si_3$	30.96	37.95	31.09	$L + \beta Nb(V)_5Si_3 \rightarrow Nb(V)Si_2 + V(Nb)_5Si_3$
	Nb-40Si-15V(A14#)	$V(Nb)_5Si_3$	60.89	36.9	2.21	$L \rightarrow \beta Nb(V)_5Si_3$
		$Nb(V)Si_2$	33.26	64.74	2	$L \rightarrow \beta Nb(V)_5Si_3 + Nb(V)Si_2$
	Nb-40Si-25V(A15#)	$\beta Nb(V)_5Si_3$	43.97	37.91	18.12	$L \rightarrow \beta Nb(V)_5Si_3$
		$V(Nb)_5Si_3$	28.75	36.63	34.63	$L \rightarrow \beta Nb(V)_5Si_3 + V(Nb)_5Si_3$
	Nb-40Si-35V(A16#)	$\beta Nb(V)_5Si_3$	33.07	37.91	29.01	$L \rightarrow \beta Nb(V)_5Si_3$
		$V(Nb)_5Si_3$	24.82	36.8	38.28	$L \rightarrow \beta Nb(V)_5Si_3 + V(Nb)_5Si_3$
		$Nb(V)Si_2$	23.5	66.2	10.3	$L + \beta Nb(V)_5Si_3 \rightarrow V(Nb)_5Si_3 + Nb(V)Si_2$
	Nb–30Si–18V(A17#)	$\beta Nb(V)_5Si_3$	52.89	37.02	10.09	$L \rightarrow \beta Nb(V)_5Si_3$
	Nb–30Si–28V(A18#)	$\beta Nb(V)_5Si_3$	45.95	37.65	16.39	$L \rightarrow \beta Nb(V)_5Si_3$
		$V(Nb)_3Si$	33.78	25.87	40.35	$L \rightarrow \beta Nb(V)_5Si_3 + V(Nb)_3Si$
	Nb-30Si-38V(A19#)	$\beta Nb(V)_5Si_3$	35.78	36.83	27.39	$L \rightarrow \beta Nb(V)_5Si_3$
		$V(Nb)_3Si$	20.81	25.34	53.86	$L \rightarrow \beta Nb(V)_5Si_3 + V(Nb)_3Si$
$V(Nb)_3Si$	Nb-20Si-65V(A20#)	$V(Nb)_3Si$	16.2	25.12	59.68	$L \rightarrow V(Nb)_3Si$
		bcc(Nb,Si,V)	17.66	6.18	76.16	$L \rightarrow V(Nb)_3Si$ + bcc(Nb,Si,V)
$(Nb,V)_2Si$	Nb-17Si-30V(A21#)	$(Nb,V)_2Si$	45.95	33.26	20.79	$L \rightarrow (Nb,V)_2Si$
		bcc(Nb,Si,V)	56.42	6.40	37.36	$L \rightarrow (Nb,V)_2Si$ + bcc(Nb,Si,V)
	Nb-20Si-45V(A22#)	$(Nb,V)_2Si$	44.53	33.86	21.61	$L \rightarrow (Nb,V)_2Si$
		$V(Nb)_3Si$	20.81	25.34	53.86	$L \rightarrow (Nb,V)_2Si + V(Nb)_3Si$
bcc(Nb,V,Si)	Nb-18Si-5V(A23#)	bcc(Nb,Si,V)	84.18	8.67	7.16	$L \rightarrow$ bcc(Nb,Si,V) + $\beta Nb(V)_5Si_3$
		$\beta Nb(V)_5Si_3$	58.25	37.8	3.95	$L \rightarrow$ bcc(Nb,Si,V) + $\beta Nb(V)_5Si_3 + Nb(V)_3Si$
		$Nb(V)_3Si$	60.12	23.86	16.2	
	Nb-10Si-35V(A24#)	bcc(Nb,Si,V)	66.54	9.32	24.14	$L \rightarrow$ bcc(Nb,Si,V)
		$(Nb,V)_2Si$	15.27	33.3	51.42	$L \rightarrow$ bcc(Nb,Si,V) + $(Nb,V)_2Si$
	Nb-15Si-20V(A25#)	bcc(Nb,Si,V)	69.6	4.84	25.56	$L \rightarrow$ bcc(Nb,Si,V)
		$\beta Nb(V)_5Si_3$	53.36	37.71	12.93	$L \rightarrow$ bcc(Nb,Si,V) + $\beta Nb(V)_5Si_{33}$

Primary phase	Nominal composition (at.%)	As-cast phases	Phase composition (at.%)			Precipitation paths
			Nb	Si	V	
	Nb-17Si-12V(A26#)	bcc(Nb,Si,V)	76.70	7.13	16.17	L → bcc(Nb,Si,V)
		$\beta Nb(V)_5Si_3$	58.55	37.29	4.16	L → bcc(Nb,Si,V) + $\beta Nb(V)_5Si_3$
	Nb-10Si-50V(A27#)	bcc(Nb,Si,V)	44.4	8.69	46.91	L → bcc(Nb,Si,V)
		$(Nb,V)_2Si$	33.57	24.76	41.91	L → bcc(Nb,Si,V) + $V(Nb)_3Si$
	Nb-10Si-50V(A28#)	bcc(Nb,Si,V)	21.59	7.88	70.53	L → bcc(Nb,Si,V)
		$(V(Nb))_3Si$	18.92	24.1	56.98	L → bcc(Nb,Si,V) + $V(Nb)_3Si$
	Nb-10Si-80V(A29#)	bcc(Nb,Si,V)	18.07	7.89	74.04	L → bcc(Nb,Si,V)
		$(V(Nb))_3Si$	9.22	25.56	65.22	L → bcc(Nb,Si,V) + $V(Nb)_3Si$

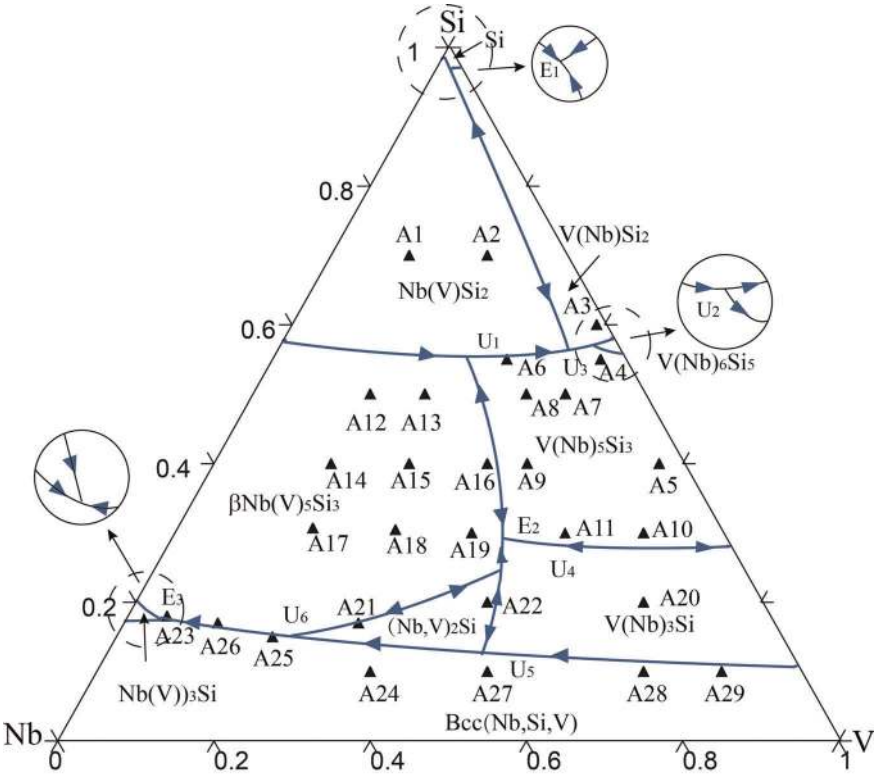

Fig. 2. Liquidus projection of the Nb–Si–V ternary system.

light gray phase around $Nb(V)Si_2$ and Diamond(Si) (the black phase). The fine eutectic structure was found in the SEM/BSE images of the alloys A1# and A2#. The solidification paths of the alloys are as follows: the white primary phase $Nb(V)Si_2$ precipitated first L → $Nb(V)Si_2$, then the light gray phase $V(Nb)Si_2$ was formed after the peritectic reaction L + $Nb(V)Si_2$ → $V(Nb)Si_2$, and finally the equilibrium eutectic reaction L → $Nb(V)Si_2$ + $V(Nb)Si_2$ + Diamond(Si) reached and the solidification came to the end.

3.1.2. The primary phases of $V(Nb)Si_2$

As is shown in Fig. 4, the SEM/BSE micrograph and the X-ray diffractogram of the as-cast alloy A3# Nb-60Si-39V indicate that its microstructure is composed of black $V(Nb)Si_2$ primary phase and the white $V(Nb)_6Si_5$ subsequently solidified phase. The solidification path of the alloy is as follows: the primary phase $V(Nb)Si_2$ first precipitated from liquid L → $Nb(V)Si_2$, then the liquid composition reached the univariant line of the eutectic reaction L → $V(Nb)Si_2$ + $V(Nb)_6Si_5$, and the liquid composition moved forward along the univariant line until the solidification process was over.

3.1.3. Primary solidification region of $V(Nb)_5Si_3$

As is shown in Fig. 5, the experimental results of the alloys A4# Nb-55Si-42V and A5# Nb-40Si-57V, indicate that

their microstructures are composed of the white $V(Nb)_5Si_3$ phase and the gray $V(Nb)Si_2$ phase. The solidification path of each alloy is as follows: the primary phase $V(Nb)_5Si_3$ first precipitated from liquid $L \rightarrow V(Nb)_5Si_3$, then the liquid composition reached the univariant line of the eutectic reaction $L \rightarrow V(Nb)Si_2 + V(Nb)_5Si_3$, and the liquid composition moved forward along the univariant line until the solidification process was over.

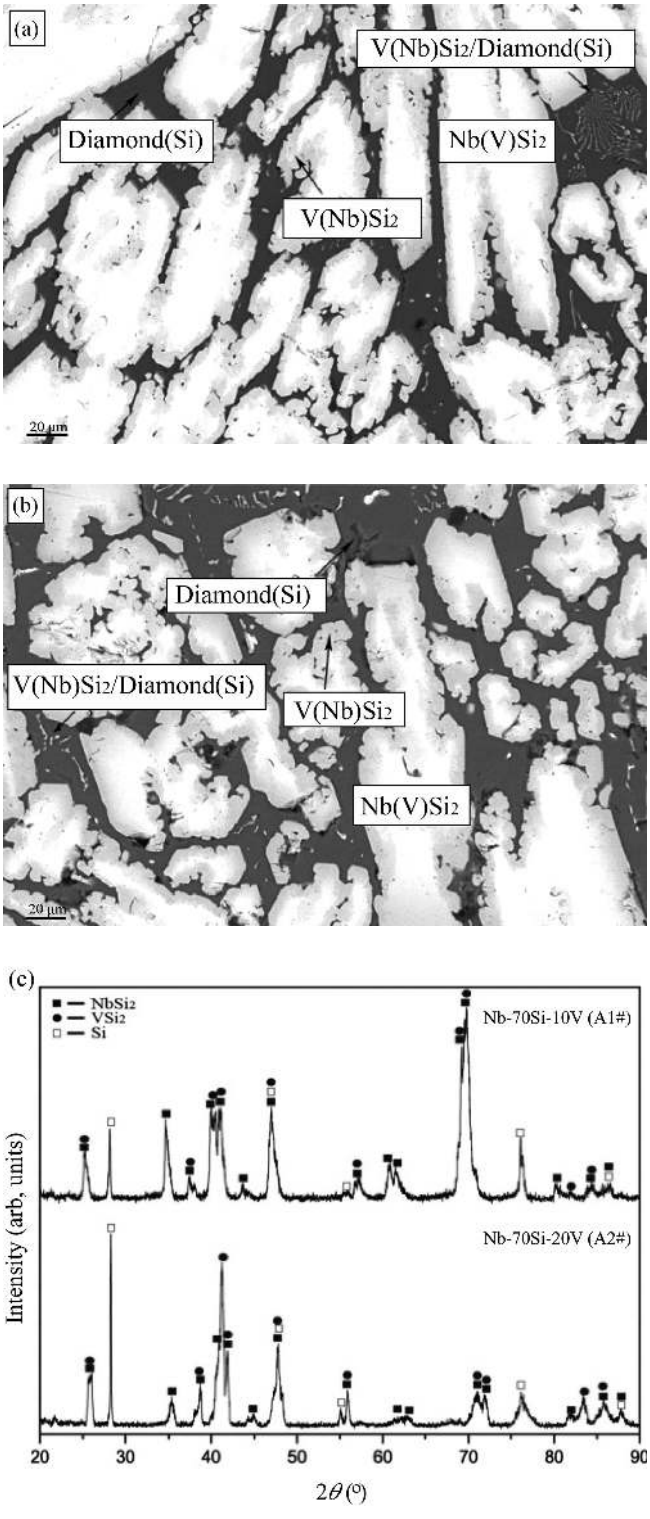

Fig. 3. SEM/BSE micrographs of (a) A1# Nb-70Si-10V, and (b) A2# Nb-70Si-20 V; (c) X-ray diffractograms.

As is shown in Fig. 6, the SEM/BSE micrograph and the X-ray diffractogram of the as-cast alloy A6# Nb-55Si-30V indicate that its microstructure is composed of the white $V(Nb)_5Si_3$ phase, the light gray $Nb(V)Si_2$ phase and the havy gray $V(Nb)Si_2$ phase. The solidification path of the alloy is as follows: the primary phase $V(Nb)_5Si_3$ first solidified from liquid $L \rightarrow V(Nb)_5Si_3$, then $V(Nb)_5Si_3$ and $Nb(V)Si_2$ solidified eutectically from liquid $L \rightarrow V(Nb)_5Si_3 + Nb(V)Si_2$, and then the liquid composition moved forward along the univariant line until reached the invariant reaction $L + Nb(V)Si_2 \rightarrow V(Nb)_5Si_3 + V(Nb)Si_2$.

As is shown in Fig. 7, the SEM/BSE micrograph and the X-ray diffractogram of the as-cast alloy A10# Nb-30Si-60V indicate that the microstructure is composed of the light gray $V(Nb)_5Si_3$ phase, the white $\beta Nb(V)_5Si_3$ phase and the heavy gray $V(Nb)_3Si$ phase. Different from the alloy A6#, the solidification path of the alloy A10# is as follows: the primary phase $V(Nb)_5Si_3$ first solidified from liquid $L \rightarrow V(Nb)_5Si_3$, then the liquid composition reached the univariant line, $L \rightarrow \beta Nb(V)_5Si_3 + V(Nb)_5Si_3$. and finally the liquid composition moved forward along the univariant line until reached the eutectic invariant reaction $L \rightarrow \beta Nb(V)_5Si_3 + V(Nb)_5Si_3 + V(Nb)_3Si$.

3.1.4. Primary solidification region of $\beta Nb(V)_5Si_3$

SEM/BSE micrographs and the X-ray diffractograms of the alloys A12# Nb-50Si-15V and A13# Nb-50Si-22V are shown in Fig. 8, indicating that the microstructures of both alloys are

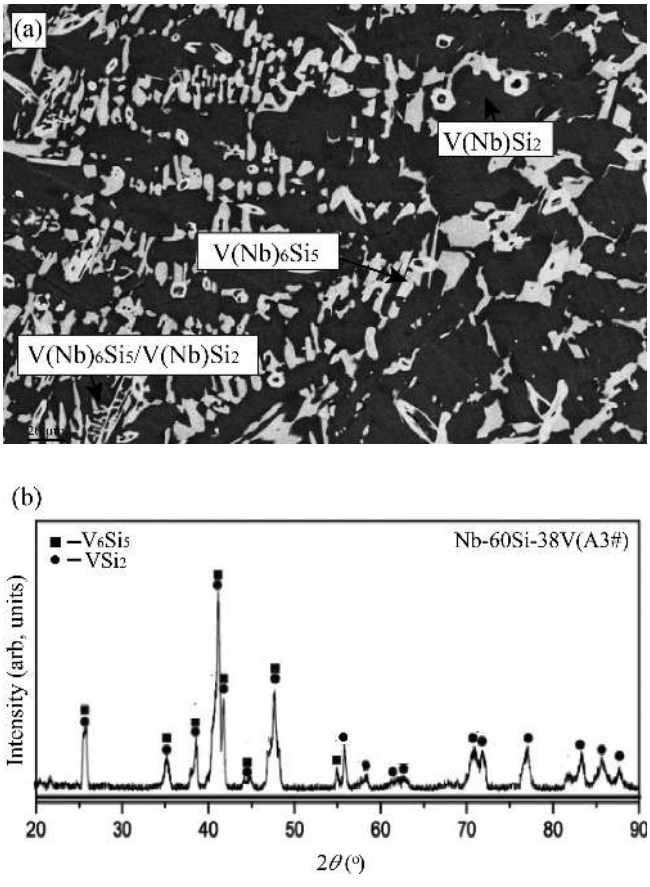

Fig. 4. (a) SEM/BSE micrograph, and (b) X-ray diffractogram of A3# Nb-60Si-39V.

composed of the white $\beta Nb(V)_5Si_3$ phase, the gray $V(Nb)_5Si_3$ phase and the dark $Nb(V)Si_2$. The solidification path is as follows: the white primary phase $\beta Nb(V)_5Si_3$ first solidified from liquid $L \rightarrow \beta Nb(V)_5Si_3$, then the composition of liquid phase moved to $L \rightarrow \beta Nb(V)_5Si_3 + Nb(V)Si_2$, and along the the univariant line the liquid composition reached the invariant reaction $L + \beta Nb(V)_5Si_3 \rightarrow V(Nb)_5Si_3 + Nb(V)Si_2$.

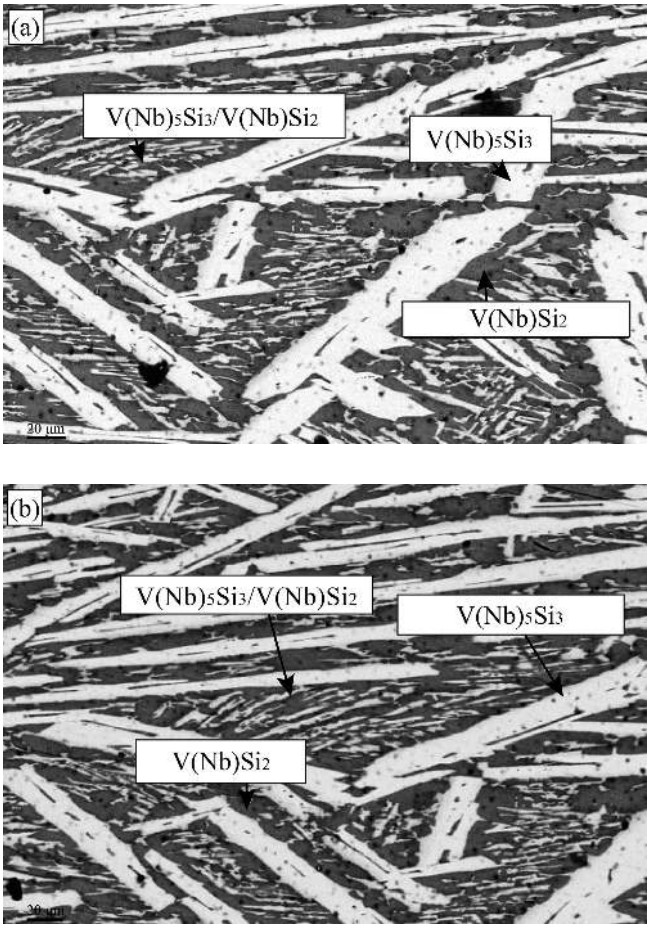

Fig. 5. SEM/BSE micrographs (a) A4# Nb-55Si-42V, and (b) A5# Nb-40Si-57V; (c) X-ray diffractograms.

As is shown in Fig. 9a, the microstructure of the alloy A14# Nb-40Si-15V is composed of the white $\beta Nb(V)_5Si_3$ phase and the gray $Nb(V)Si_2$ phase. Both the phases $\beta Nb(V)_5Si_3$ and $Nb(V)Si_2$ form the typical eutectic micro-

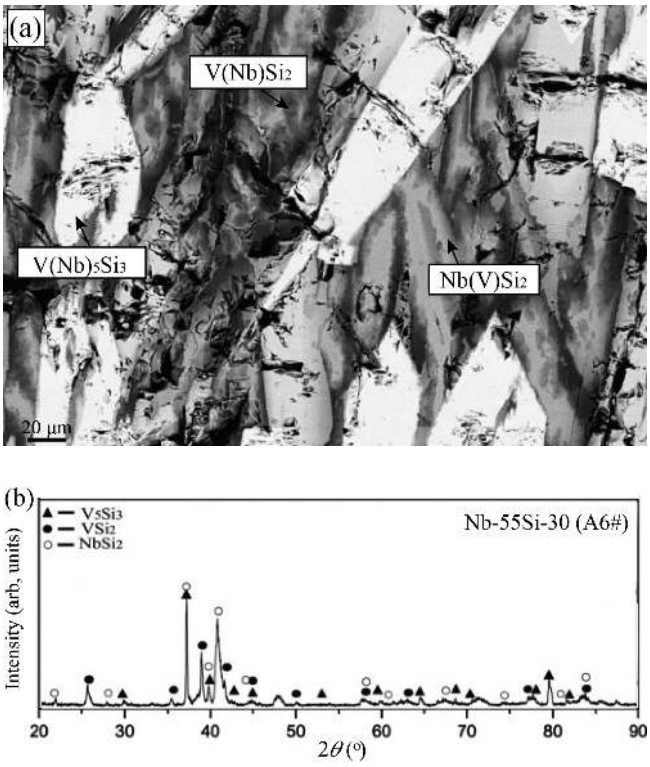

Fig. 6. (a) SEM/BSE micrograph, and (b) X-ray diffractogram of A6# Nb-55Si-30V.

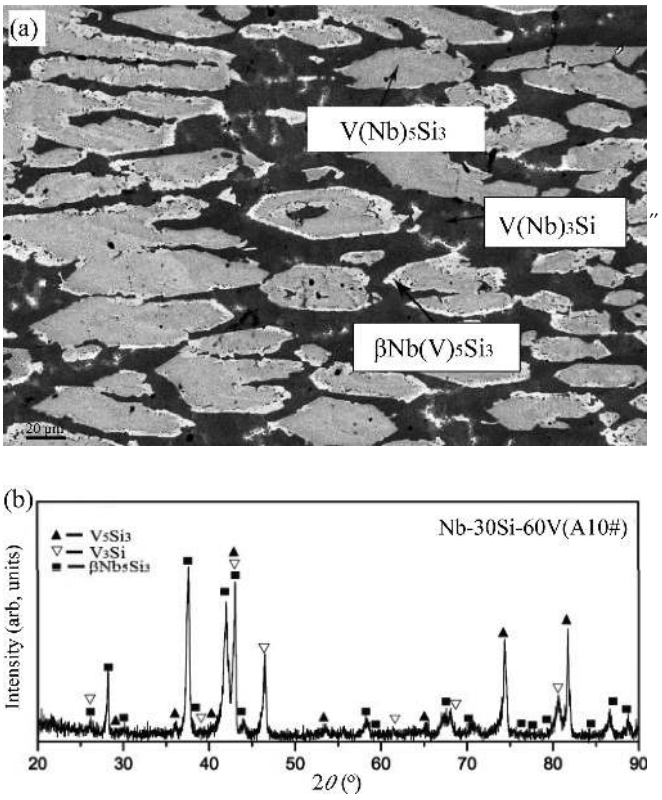

Fig. 7. (a) SEM/BSE micrograph, and (b) X-ray diffractogram of A10# Nb-30Si-60V.

structure. Therefore, the solidification path of the alloy A14# is as follows: the primary phase $\beta Nb(V)_5Si_3$ first solidified from liquid $L \rightarrow \beta Nb(V)_5Si_3$, and then the liquid composition reached the univariant line $L \rightarrow \beta Nb(V)_5Si_3 + Nb(V)Si_2$. The microstructure of the alloy A16# Nb-40Si-35V, as shown in Fig. 9b, is composed of the white $\beta Nb(V)_5Si_3$ phase, the light gray $V(Nb)_5Si_3$ phase and the heavy gray $Nb(V)Si_2$ phase. Different from that of the alloy A14#, the solidification path of the alloy A16# is as follows: the primary phase $\beta Nb(V)_5Si_3$ first solidified from liquid $L \rightarrow \beta Nb(V)_5Si_3$, then the liquid composition moved to the univariant line, $L \rightarrow \beta Nb(V)_5Si_3 + V(Nb)_5Si_3$, along which the liquid composition reached the invariant reaction $L + \beta Nb(V)_5Si_3 \rightarrow V(Nb)_5Si_3 + Nb(V)Si_2$.

SEM/BSE micrographs and the X-ray diffractograms of the alloys A17# Nb-30Si-18V and A18# Nb-30Si-28V are shown

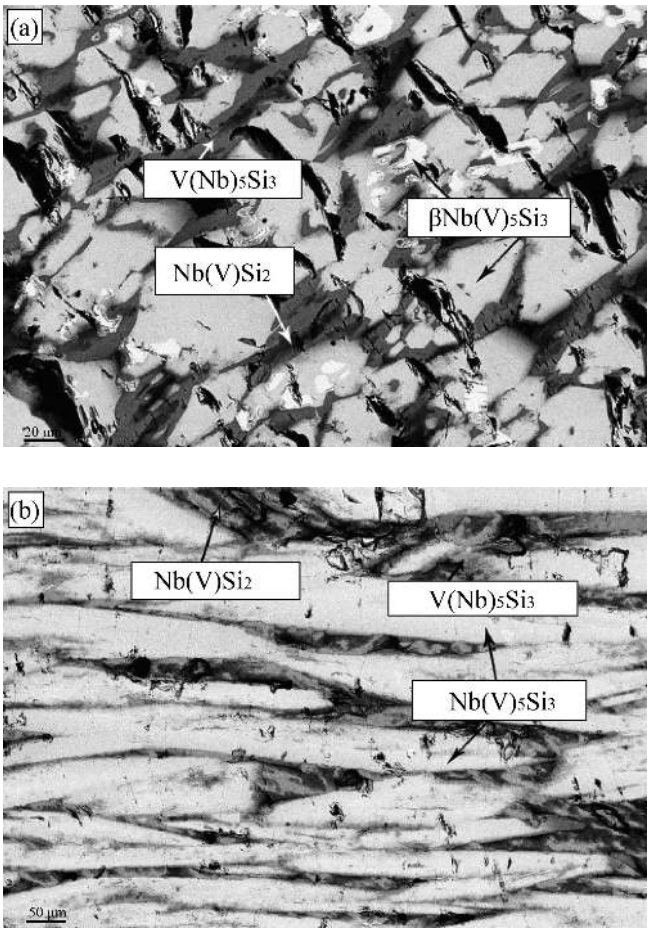

Fig. 8. SEM/BSE micrographs of (a) A12# Nb-50Si-15V, and (b) A13# Nb-50Si-22 V; (c) X-ray diffractograms.

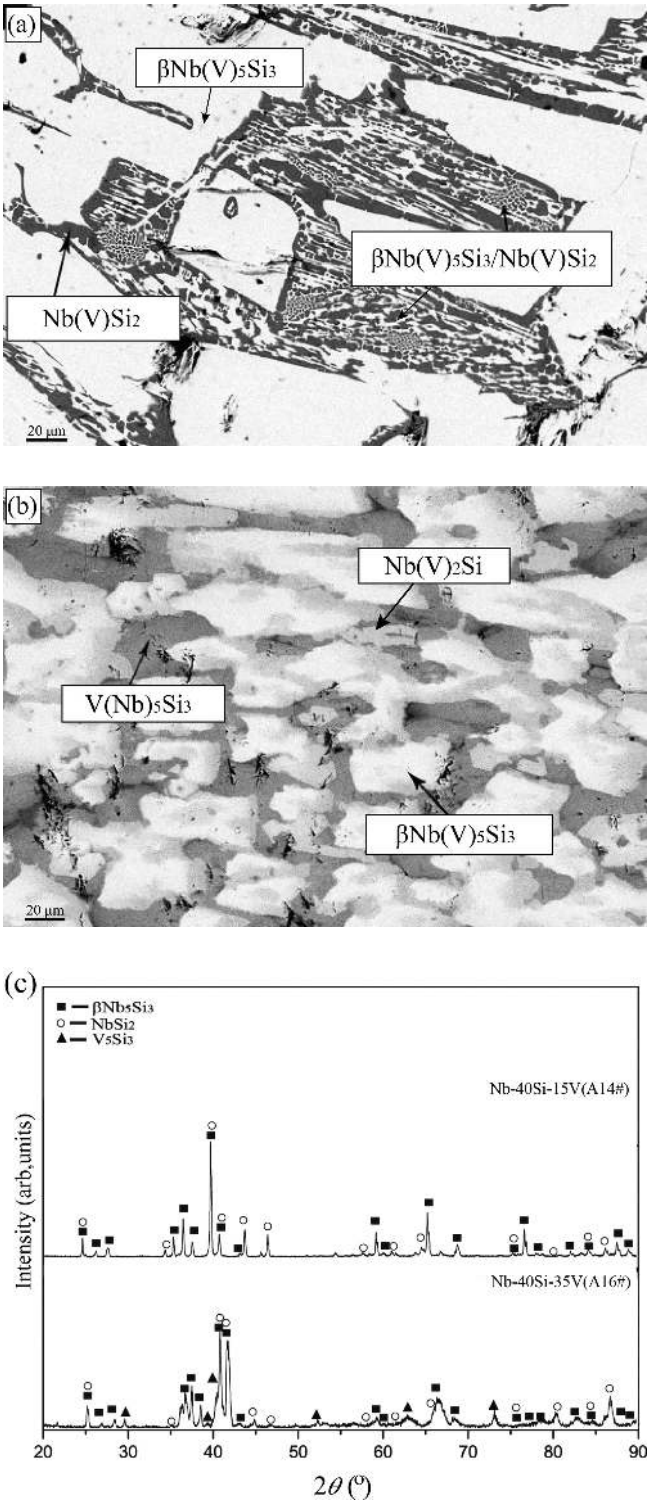

Fig. 9. SEM/BSE micrographs of (a) A14# Nb-40Si-15V, and (b) A16# Nb-40Si-35V; (c) X-ray diffractograms.

in Fig. 10. The major constituent phase of the alloy A17# is $\beta Nb(V)_5Si_3$, as shown in Fig. 10a. The microstructure of the alloy A18# is composed of the white primary phase $\beta Nb(V)_5Si_3$ and the eutectic structure formed by the two phases $\beta Nb(V)_5Si_3$ (the white phase) and $V(Nb)_3Si$ (the gray phase).

3.1.5. Primary solidification region of $V(Nb)_3Si$

As is shown in Fig. 11, the microstructure of A20# Nb-20Si-65V is composed of the dark gray primary phase $V(Nb)_3Si$ and the eutectic structure formed by the two phases $V(Nb)_3Si$ (the dark gray phase) and Bcc(Nb,Si,V) (the white phase).

3.1.6. Primary solidification region of $(Nb,V)_2Si$

The SEM/BSE micrographs of A21# Nb-17Si-30V and A22# Nb-20SiV-45V are shown in Fig. 12. The microstructure of the alloy A21# is composed of the gray primary phase $(Nb,V)_2Si$ and the eutectic structure formed by the two phases $(Nb,V)_2Si$ (the gray phase) and bcc(Nb,Si,V) (the white phase). It is very important to note that the newly discovered ternary linear compound $(Nb,V)_2Si$ has been reported in the previous study of Li et al. [17] and has been found in both the as-cast and the isothermal alloys in the present work. This compound has a stoichiometric ratio of 2 : 1 for (Nb,V) : Si, while its refined crystal structure has not been reported yet. The microstructure of the alloy A22# is composed of the primary white phase $(Nb,V)_2Si$ and the eutectic structure formed by the two phases $(Nb,V)_2Si$ (the white phase) and bcc(Nb,Si,V) (the gray phase).

3.1.7. Primary solidification region of bcc(Nb,Si,V)

SEM/BSE morphologies and X-ray diffractograms for the alloys A25# Nb-15Si-20V and A26# Nb-17Si-12V are shown in Fig. 13. The microstructures of both the alloys A25# and A26# are composed of the white primary phase bcc(Nb,Si,V), and the eutectic structure formed by the two phases bcc(Nb,Si,V) (the white phase) and $\beta Nb(V)_5Si_3$. (the gray phase). The microstructure of the alloy A23# Nb-18Si-5V, as

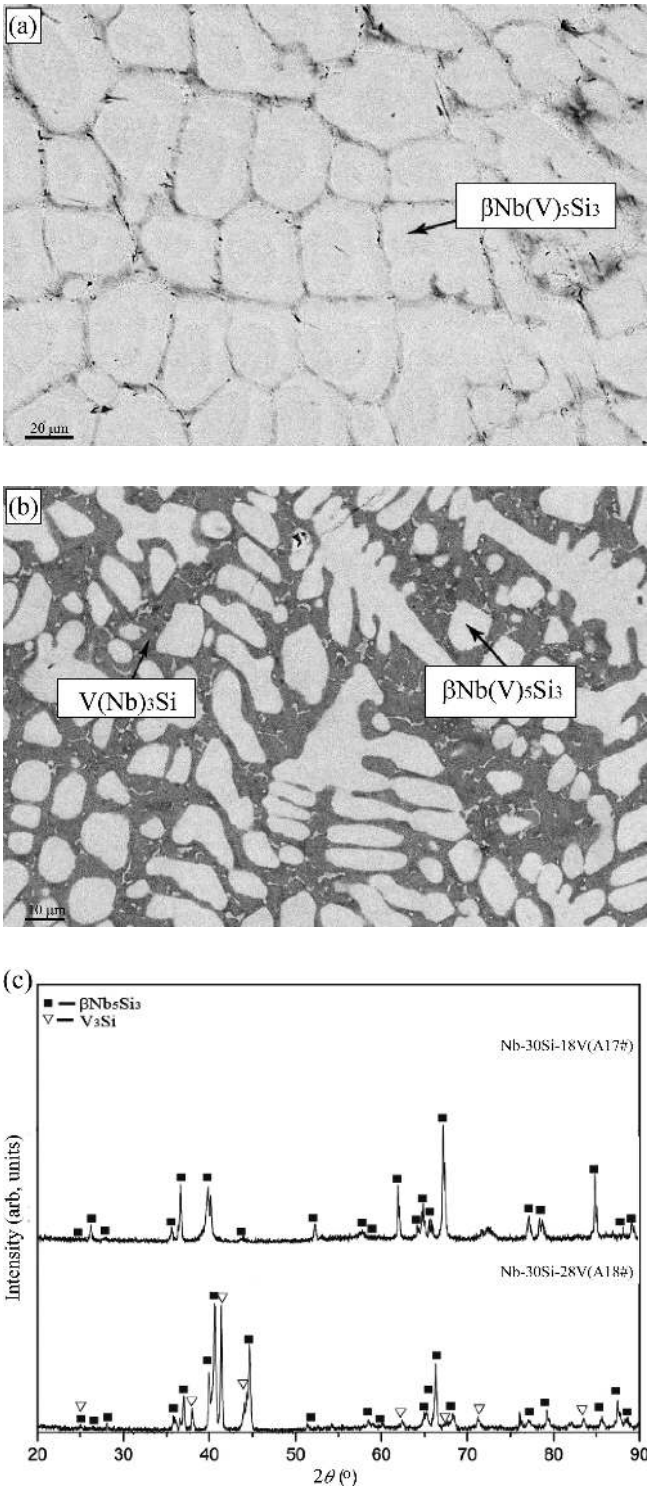

Fig. 10. SEM/BSE micrographs of (a) A17# Nb-30Si-18V, and (b) A18# Nb-30Si-28V; (c) X-ray diffractograms.

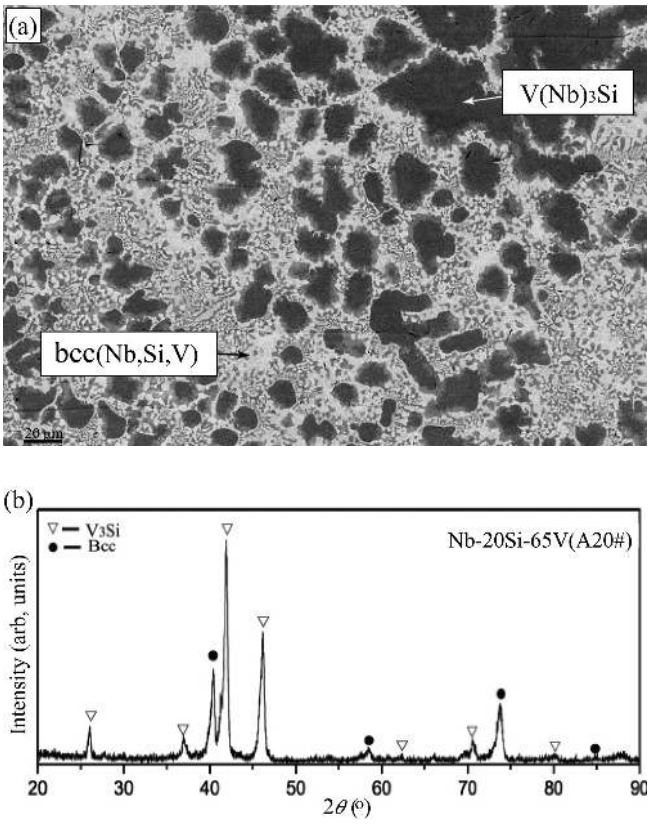

Fig. 11. (a) SEM/BSE micrograph, and (b) X-ray diffractogram of A20# Nb-20Si-65V.

shown in Fig. 14, is composed of the fine binary eutectic structure formed by the two phases Bcc(Nb,Si,V) (the white phase) and $\beta Nb(V)_5Si_3$ (the gray phase), and the even more fine ternary eutectic structure formed by the three phases bcc(Nb,Si,V) (the white phase), $\beta Nb(V)_5Si_3$ (the gray phase) and $Nb(V)_3Si$ (the phase indicated by XRD diffractogram).

The microstructure of the alloy A24# Nb-10Si-35V is composed of the white primary phase bcc(Nb,Si,V) and the black phase $(Nb,V)_2Si$. The precipitation path of the alloy A24# is that the white phase bcc(Nb,Si,V) is first precipitated from liquid. Then the liquid composition reached the univariant line, $L \rightarrow (Nb,V)_2Si$ + bcc(Nb,Si,V).

The X-ray diffractograms and BSE micrographs of Nb-10Si-(50,80)V (A27#,A29#) alloys are shown in Fig. 15. The microstructures of the alloys are all gray-white lamellar eutectic structures of bcc(Nb,Si,V)/$V(Nb)_3Si$. The nominal compositions of the alloys are all very close to the univariant line of bcc(Nb,Si,V)/$V(Nb)_3Si$.

3.2. Experimental results of the isothermal section at 1 300 °C

After 20 days of isothermal treatment at 1 300 °C, the constituent phases and their equilibria compositions of the Nb–Si–V alloys were measured by SEM and EMPA methods respectively and are listed in Table 3. With the combination of the experimental data and the preliminarily optimized results, eight three-phase regions and thirteen two-phase regions were observed in the isothermal section at 1 300 °C. The three-phase regions are as follows: $Nb(V)Si_2$ + $V(Nb)Si_2$ + Diamond(Si), $Nb(V)Si_2$ + $V(Nb)Si_2$ + $V(Nb)_6Si_5$, $Nb(V)Si_2$ + $\alpha Nb(V)_5Si_3$ + $V(Nb)_6Si_5$, $V(Nb)_5Si_3$ + $\alpha Nb(V)_5Si_3$ + $V(Nb)_6Si_5$, $V(Nb)_5Si_3$ + $\alpha Nb(V)_5Si_3$ + $(Nb,V)_2Si$, bcc(Nb,Si,V) + $\alpha Nb(V)_5Si_3$ + $(Nb,V)_2Si$, $V(Nb)_5Si_3$ + $V(Nb)_3Si$ + $(Nb,V)_2Si$, bcc(Nb,Si,V) + $V(Nb)_3Si$ + $(Nb,V)_2Si$. The experimental determined isothermal sections of 1 300 °C is shown in Fig. 16.

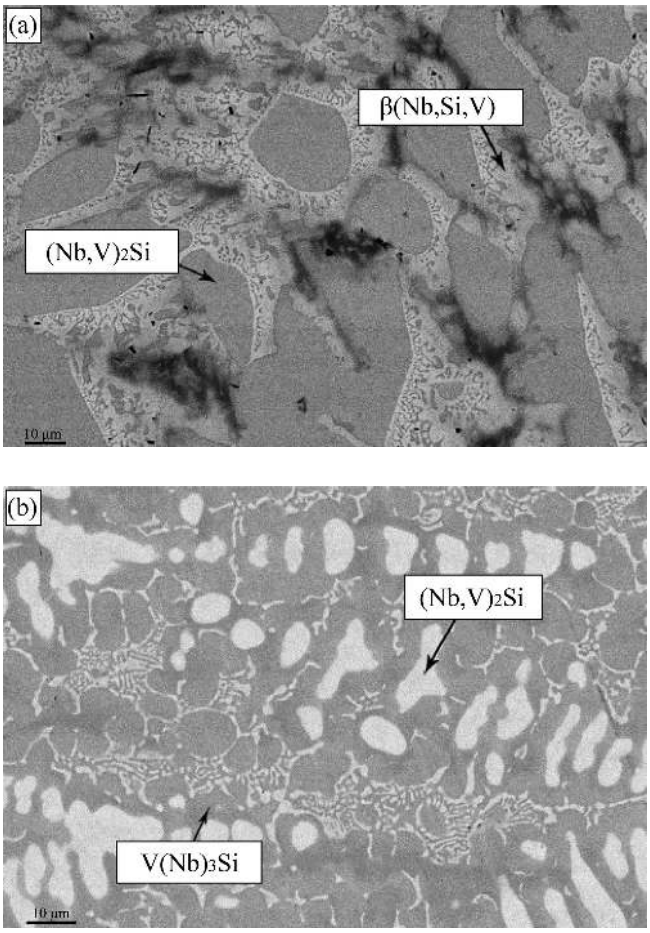

Fig. 12. SEM/BSE micrographs of (a) A21# Nb-17Si-30 V, and (b) A22# Nb-20Si-45 V.

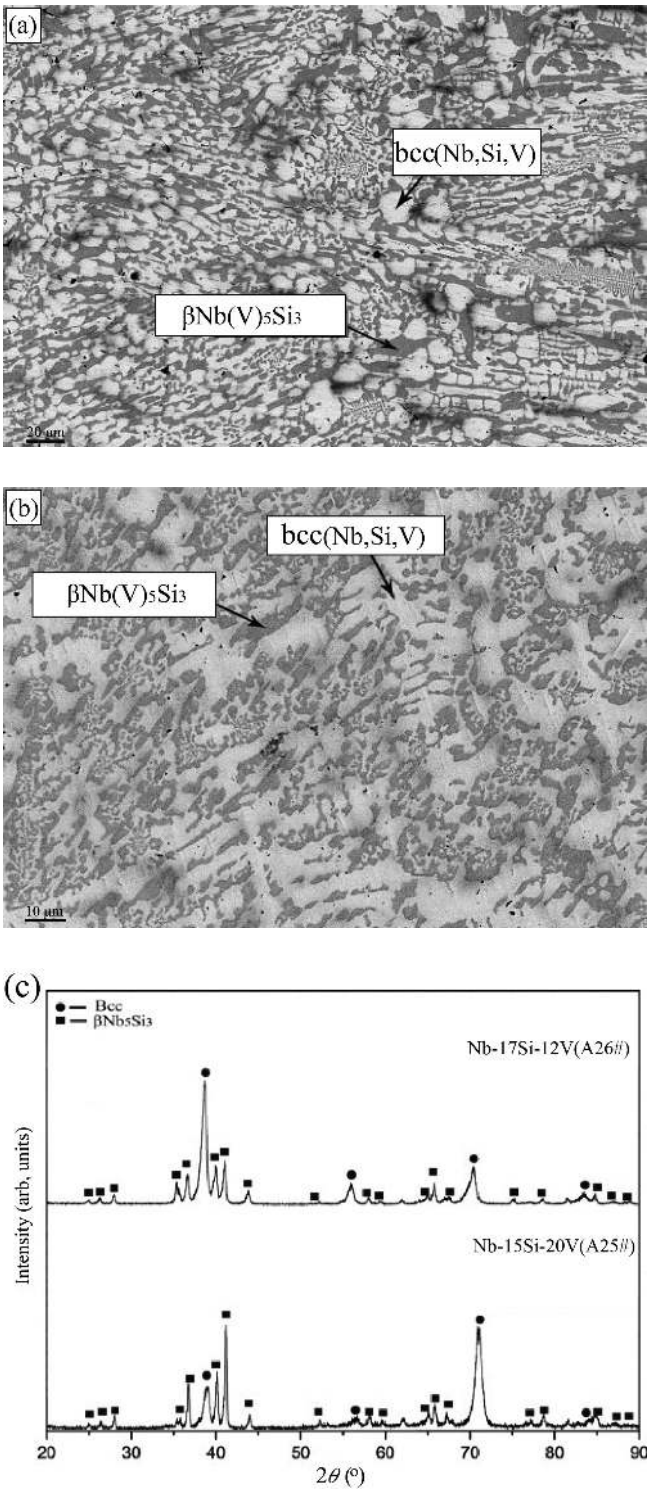

Fig. 13. SEM/BSE micrographs of (a) A25# Nb-15Si-20V, and (b) A26# Nb-17Si-12V; (c) X-ray diffractograms.

3.2.1. Phase equilibria related to $Nb(V)Si_2$ and $V(Nb)Si_2$

As is shown in Fig. 17, the equilibrium microstructure of the alloy B2# Nb-70Si-20V is composed of the black phase Diamond(Si), the white phase $Nb(V)Si_2$ and the gray phase $V(Nb)Si_2$, constituting the three-phase region $Nb(V)Si_2$ + $V(Nb)Si_2$ + Diamond(Si). Meanwhile, as is shown in Fig. 18, the SEM/BSE micrograph and X-ray diffractogram indicate that the equilibrium microstructure of the alloy B3# Nb-50Si-20V is composed of the black phase $V(Nb)Si_2$, the gray phase $Nb(V)Si_2$ and the white phase $V(Nb)_6Si_5$, constituting the three-phase region

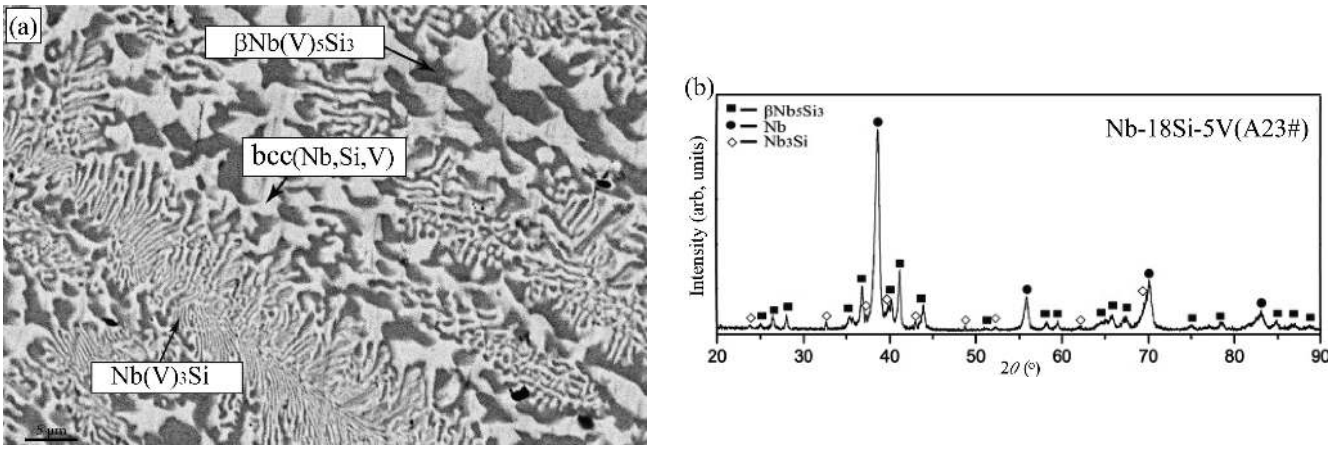

Fig. 14. (a) SEM/BSE micrograph, and (b) X-ray diffractogram of A23# Nb-18Si-5V.

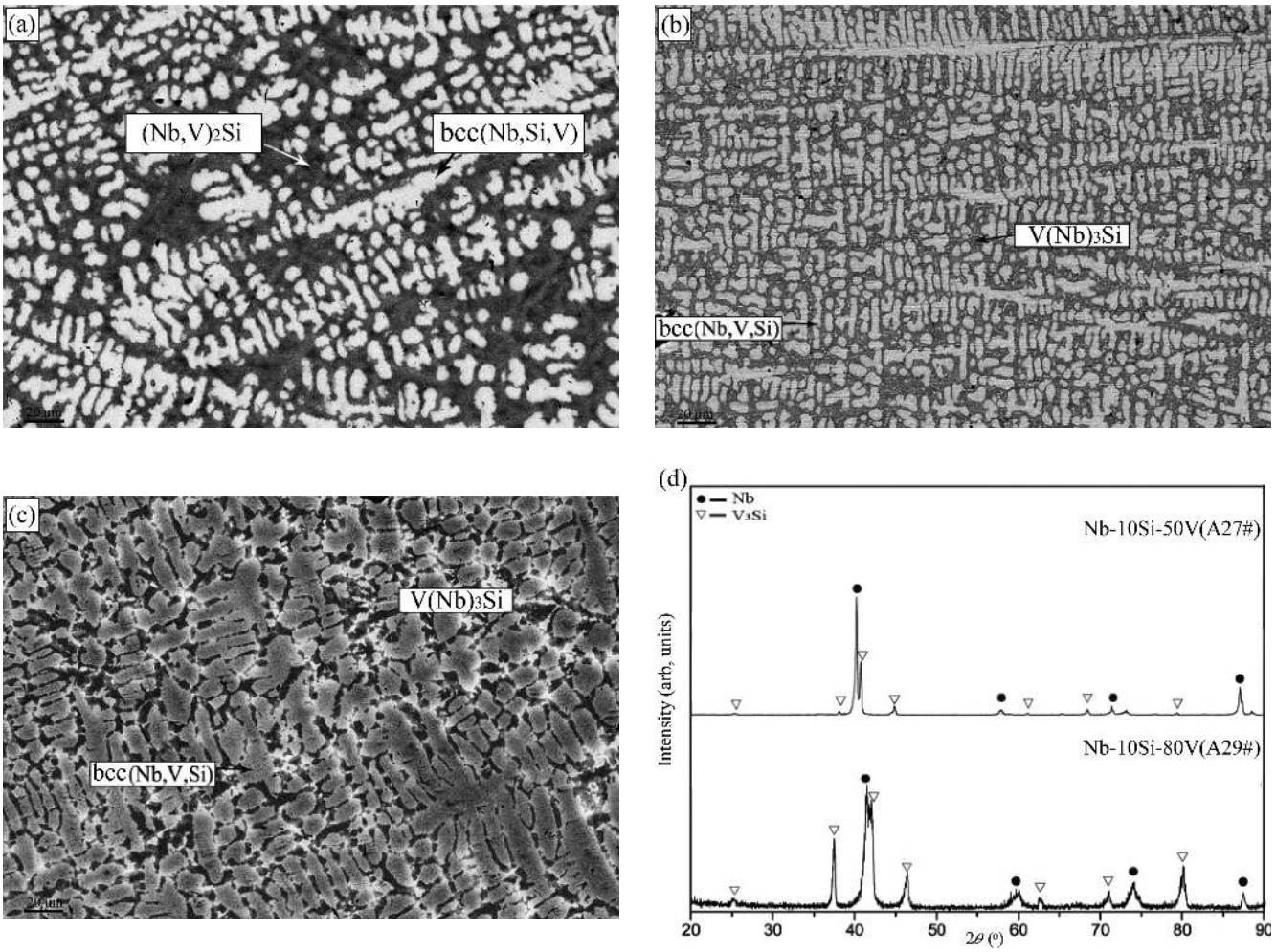

Fig. 15. SEM/BSE micrographs of (a) A24# Nb-10Si-35V, (b) A27# Nb-10Si-50V, (c) A29# Nb-10Si-80V, and X-ray diffractograms of (d) Nb-10Si-(50,80)V (A27#, A29#).

Table 3. Constituent phases and their equilibrium compositions of the heat-treated alloys.

Nominal composition (at.%)	Equilibrated Phases	Phase compositions (at.%)								
		Phase 1			Phase 2			Phase 3		
		Nb	Si	V	Nb	Si	V	Nb	Si	V
(B1#) Nb-70Si-10V	$Nb(V)Si_2$ + $V(Nb)Si_2$ + Diamond(Si)	24.0	67.2	8.8	12.2	67.1	20.7	99.6	0.3	0.1
(B2#) Nb-70Si-20V	$Nb(V)Si_2$ + $V(Nb)Si_2$ + Diamond(Si)	23.0	67.3	9.7	8.9	68.4	22.7	0.6	99.1	0.3
(B3#) Nb-55Si-30V	$Nb(V)Si_2$ + $V(Nb)Si_2$ + $V(Nb)_6Si_5$	22.7	67.0	10.3	9.5	67.2	23.3	14.0	45.7	40.3
(B4#) Nb-50Si-20V	$Nb(V)Si_2$ + $V(Nb)_6Si_5$ + $\alpha Nb(V)_5Si_3$	25.9	67.1	7.0	25.0	45.2	29.8	41.8	38.4	19.8
(B5#) Nb-40Si-30V	$V(Nb)_6Si_5$ + $V(Nb)_5Si_3$ + $\alpha Nb(V)_5Si_3$	21.2	45.6	33.2	15.5	39.0	45.5	32.5	39.5	28.0
(B6#) Nb-40Si-40V	$V(Nb)_6Si_5$ + $V(Nb)_5Si_3$ + $\alpha Nb(V)_5Si_3$	19.5	45.7	34.8	15.1	39.0	45.9	30.6	39.1	30.3
(B7#) Nb-40Si-4V	$Nb(V)Si_2$ + $\alpha Nb(V)_5Si_3$	29.1	66.9	4.0	56.0	37.8	4.2	–	–	–
(B8#) Nb-50Si-30V	$Nb(V)Si_2$ + $V(Nb)_6Si_5$	22.3	68.1	9.6	17.0	45.6	37.4			
(B9#) Nb-60Si-39V	$V(Nb)Si_2$ + $V(Nb)_6Si_5$	0.6	65.5	33.9	1.8	46.8	51.4			
(B10#) Nb-50Si-40V	$V(Nb)Si_2$ + $V(Nb)_6Si_5$	3.4	65.2	31.4	12.1	45.8	42.1			
(B11#) Nb-40Si-25V	$V(Nb)_6Si_5$ + $\alpha Nb(V)_5Si_3$	21.9	45.6	32.5	37.6	38.6	23.8			
(B12#) Nb-30Si-68V	$V(Nb)_3Si$ + $V(Nb)_5Si_3$	0.5	26.5	73.0	4.0	38.1	57.9			
(B13#) Nb-30SI-20V	bcc(Nb,Si,V) + $\alpha Nb(V)_5Si_3$ + $(Nb,V)_2Si$	68.8	1.6	37.6	50.9	37.3	11.4	41.7	33.6	24.7
(B14#) Nb-30Si-48V	$V(Nb)_5Si_3$ + $(Nb,V)_2Si$ + $V(Nb)_3Si$	14.3	36.5	49.2	39.9	33.0	28.1	7.9	26.4	70.7
(B15#) Nb-20Si-60V	$(Nb,V)_2Si$ + V(Nb)3Si + bcc(Nb,Si,V)	34.5	33.8	31.7	20.6	21.5	57.9	18.6	2.0	79.4
(B16#) Nb-20Si-40V	bcc(Nb,Si,V) + $(Nb,V)_2Si$	39.5	1.9	58.6	38.4	33.7	27.9			

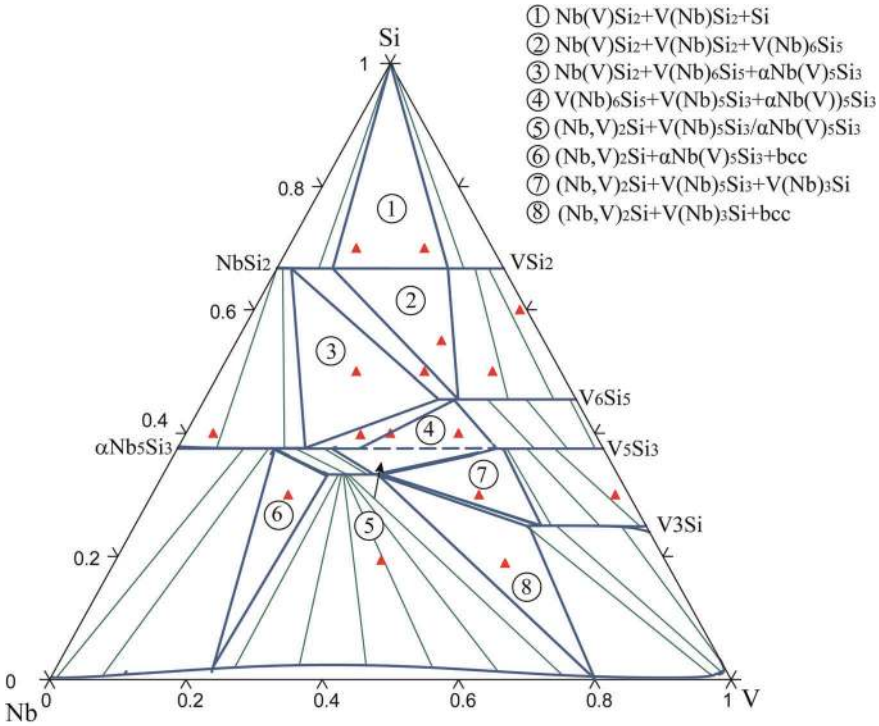

Fig. 16. Experimentally determined isothermal sections of 1 300 °C.

$Nb(V)Si_2 + V(Nb)Si_2 + V(Nb)_6Si_5$. Figure 19 shows the SEM/BSE micrograph and X-ray diffractogram of the alloy B4# Nb-50Si-20V, in the three-phase region $\alpha Nb(V)_5Si_3 + V(Nb)_6Si_5 + Nb(V)Si_2$.

3.2.2. Phase equilibrium related to $(Nb,V)_2Si$

SEM/BSE micrographs of the heat-treated alloys B13# Nb-30Si-20V, B14# Nb-30Si-48V and B15# Nb-20Si-60V are shown in Fig. 20, in which the $(Nb,V)_2Si$ phase was observed. The microstructure of the alloy B13# is composed of the white phase bcc(Nb,V,Si), the gray phase $\alpha Nb(V)_5Si_3$ and the dark gray phase $(Nb,V)_2Si$. That of

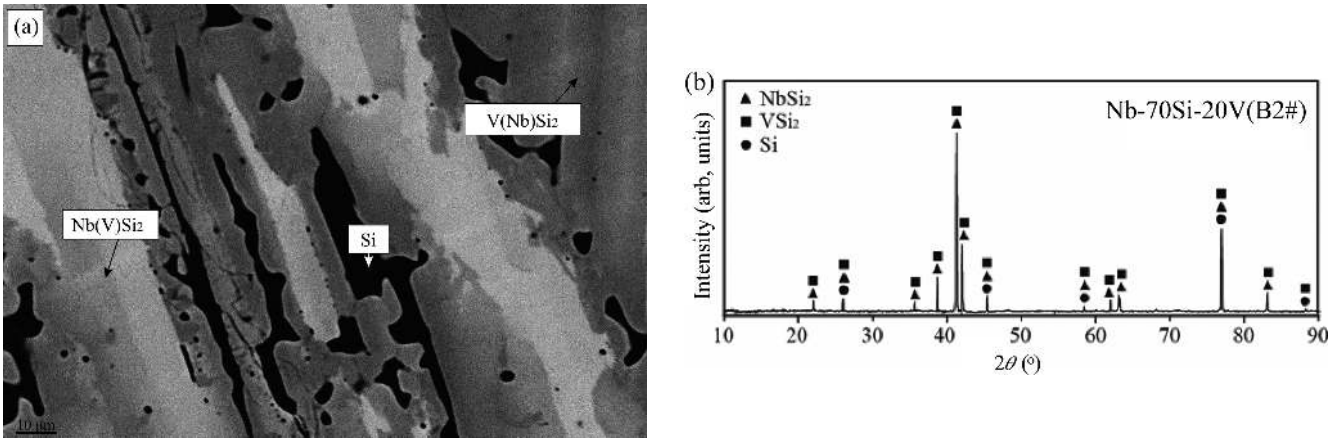

Fig. 17. (a) SEM/BSE micrograph, and (b) X-ray diffractogram of B2# Nb-70Si-20V.

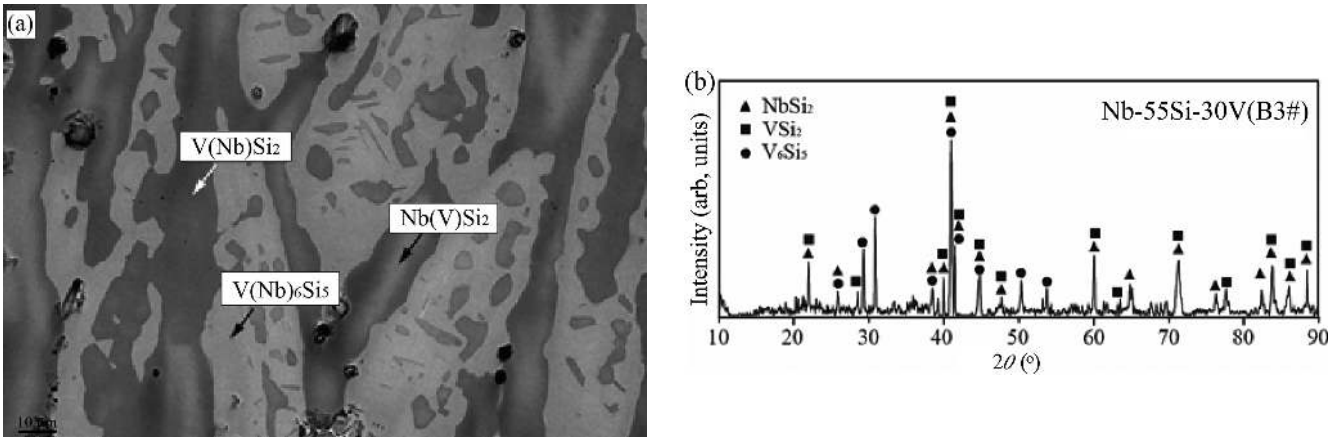

Fig. 18. (a) SEM/BSE micrograph, and (b) X-ray diffractogram of B3# Nb-55Si-30V.

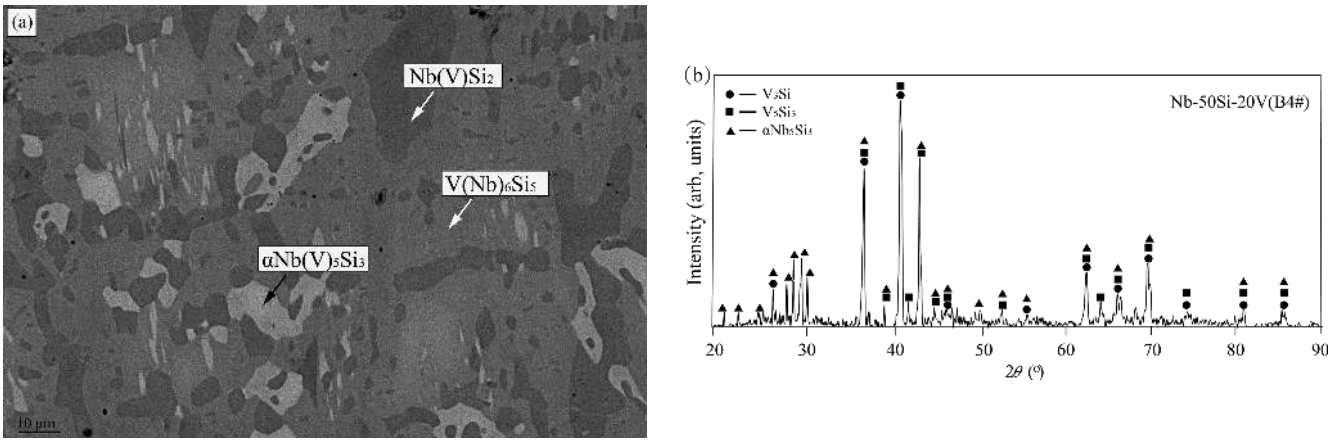

Fig. 19. (a) SEM/BSE micrograph, and (b) X-ray diffractogram of B4# Nb-50Si-20V.

the alloy B14# is composed of the white phase $V(Nb)_5Si_3$, the light gray phase $V(Nb)_3Si$ and the dark gray phase $(Nb,V)_2Si$, and that of B15# is composed of the white phase $(Nb,V)_2Si$, the black phase $V(Nb)_3Si$ and the gray phase bcc(Nb,V,Si). Therefore, the three-phase regions related to the phase $(Nb,V)_2Si$ include bcc(Nb,V,Si) + $\alpha Nb(V)_5Si_3$ + $(Nb,V)_2Si$, $V(Nb)_5Si_3$ + $V(Nb)_3Si$ + $(Nb,V)_2Si$, bcc(Nb,V,Si) + $V(Nb)_3Si$ + $(Nb,V)_2Si$. Since the crystal structure of the phase $(Nb,V)_2Si$ has not been refined, there is no standard XRD spectrum available to characterize it.

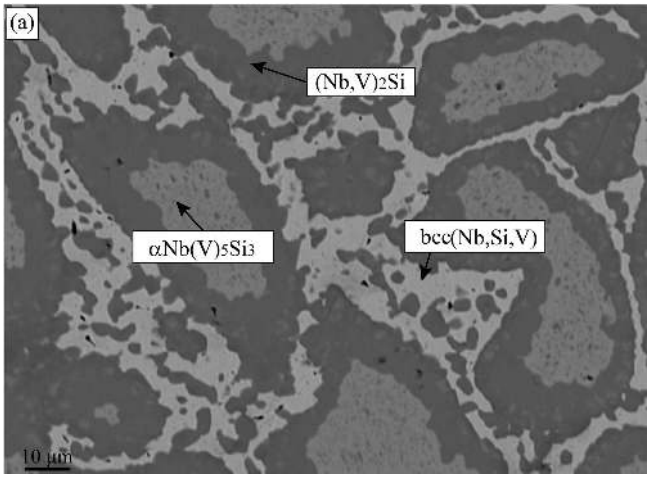

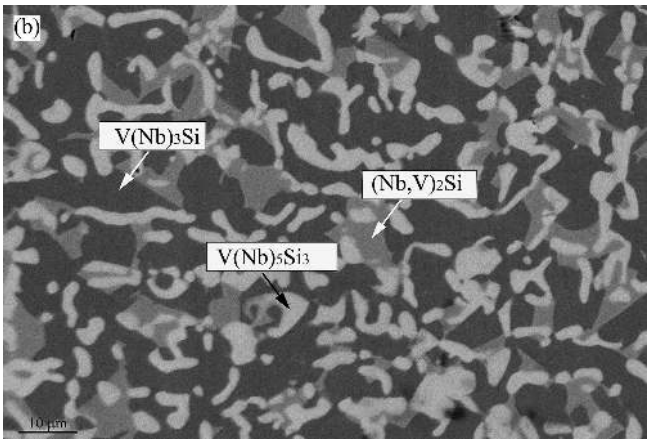

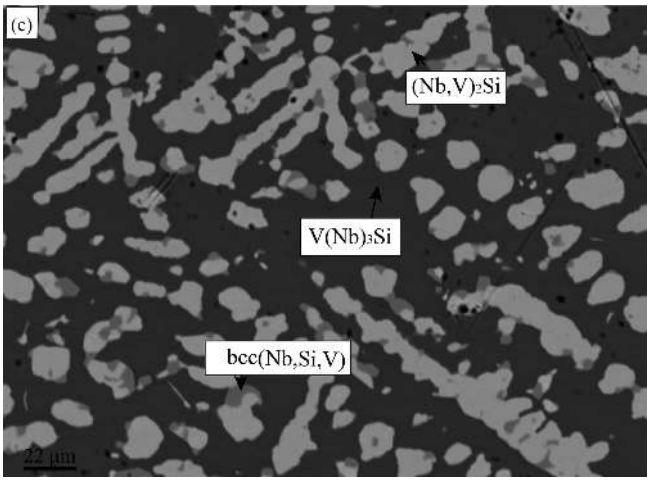

Fig. 20. SEM/BSE micrographs of the heat-treated (a) B13# Nb-30SI-20V, (b) B14# Nb-30Si-48V, and (c) B15# Nb-20Si-60V.

3.2.3. Phase equilibrium related to Nb(V)5Si3 and V(Nb)5Si3

As is shown in Fig. 21, the equilibrium microstructures of the alloys B5# Nb-40Si-30V and B6# Nb-40Si-40V are composed of the black phase $V(Nb)_6Si_5$, the gray phase $\alpha Nb(V)_5Si_3$ and the dark gray phase $V(Nb)_5Si_3$, constituting the three-phase region $V(Nb)_6Si_5$ + $\alpha Nb(V)_5Si_3$ + $V(Nb)_5Si_3$. According to the 3 three-phase regions $V(Nb)_6Si_5$ +

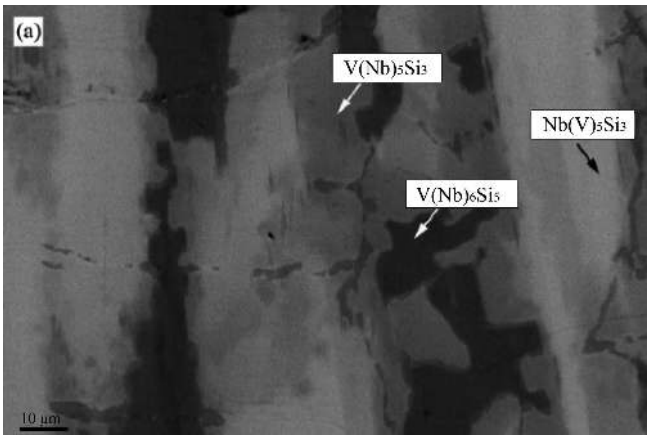

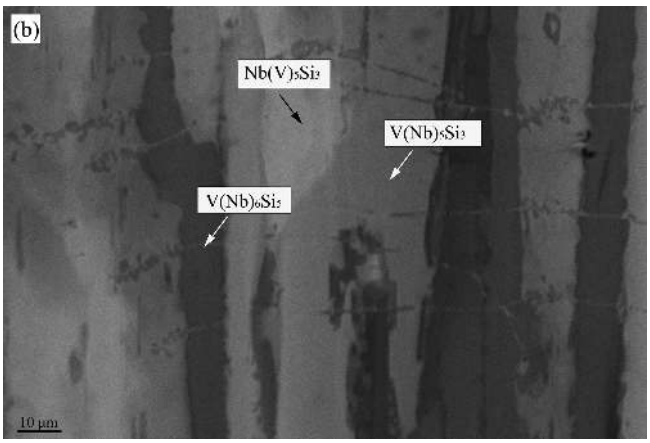

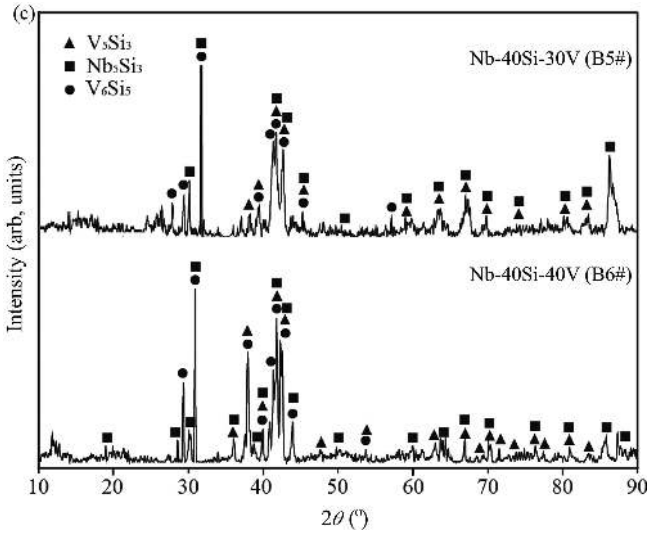

Fig. 21. SEM/BSE micrographs of (a) B5# Nb-40Si-30V, and (b) B6# Nb-40Si-40V; (c) X-ray diffractograms.

$\alpha Nb(V)_5Si_3$ + $V(Nb)_5Si_3$, bcc(Nb,V,Si) + $\alpha Nb(V)_5Si_3$ + $(Nb,V)_2Si$ and $V(Nb)_5Si_3$ + $V(Nb)_3Si$ + $(Nb,V)_2Si$, the fourth three-phase region $\alpha Nb(V)_5Si_3$ + $V(Nb)_5Si_3$ + $(Nb,V)_2Si$ can be deduced.

4. Conclusion

The liquid phase projection and the isothermal section at 1 300 °C of the Nb–Si–V ternary system have been experimentally studied by means of SEM/BSE, XRD and EPMA for observing the microstructures, identifying the constituent phases and measuring the phase compositions, respectively. The microstructures and the precipitation paths of the as-cast alloys were analyzed for constructing the liquid phase projection. The constituent phases and the related equilibrium compositions are characterized for determining the isothermal section. The existence of the linear compound $(Nb,V)_2Si$ was confirmed in studying both the liquid phase projection and the isothermal section at 1 300 °C. Together with the literature reports, the present work outlines the phase relations in the temperature–composition space of the Nb–Si–V ternary system.

This work was supported by National Key Research and Development Program of China (No. 2016YFB0701201) and National Natural Science Foundation of China (No. 51571019). Special thanks are given to the Thermo-Calc software from Thermo-Calc AB, Sweden and Pandat program licensed from The CompuThermo LLC, USA.

References

[1] J. Sha, H. Hirai, T. Tabaru, A. Kitahara, H. Ueno, S. Hanada: Mater. Sci. Eng. A 364 (2004) 151. DOI:10.1016/j.msea.2003.08.014
[2] B.P. Bewlay, M.R. Jackson, P.R. Subramanian, J.-C. Zhao: Metall. Mater. Trans. A 34 (2003) 2043. DOI:10.1007/s11661-003-0269-8
[3] Y.X. Tian, J.T. Guo, L.Y. Sheng, G.M. Cheng, L.Z. Zhou, L.L. He, H.Q. Ye: Intermetallics 16 (2008) 807. DOI:10.1016/j.intermet.2008.03.005
[4] W.Y. Kim, H. Tanaka, S. Hanada: Intermetallics 10 (2002) 625. DOI:10.1016/S0966-9795(02)00041-9
[5] K.S. Chan: Mater. Sci. Eng. A 329 (2002) 513. DOI:10.1016/S0921-5093(01)01502-7
[6] W.Y. Kim, I.D. Yeo, T.Y. Ra, G.S. Cho, M.S. Kim: J. Alloys Compd. 364 (2004) 192. DOI:10.1016/S0925-8388(03)00495-X
[7] Y.W. Kang, S.Y. Qu, J.X. Song, Y.F. Han: J. Aeronaut. Mater. 28 (2008) 6. DOI:10.3969/j.issn.1005-5053.2008.05.002
[8] Y. Kang, S. Qu, J. Song, Rare Metal Met. Eng. 38 (2009) 54. DOI:10.3321/j.issn:1002-185X.2009.z3.014
[9] W.Y. Kim, H.S. Kim, S.K. Kim, T.Y. Ra, M.S. Kim: Mater. Sci. Forum, 486 (2005) 4. DOI:10.4028/www.scientific.net/MSF.486-487.342
[10] T. Geng, C.R. Li, X.Q. Zhao, H.B. Xu, Z.M. Du, C.P. Guo: Calphad. 34 (2010) 363. DOI:10.1016/j.calphad.2010.07.003
[11] C. Zhang, D. Yong, X. Wei, H.H. Xu, P. Nash, Y.F. Ouyangc, R.X. Hu: Calphad. 32 (2008) 320. DOI:10.1016/j.calphad.2007.12.005
[12] C. Zhang, J. Wang, Y. Du, W.Q. Zhang: J. Mater. Sci. 42 (2007) 7046. DOI:10.1007/s10853-007-1865-6
[13] K.C. Hari Kumar, P. Wollants, L. Delaey: Calphad. 18 (1994) 71. DOI:10.1016/0364-5916(94)90008-6
[14] J.T. Gao, C.R. Li, C.P. Guo, Z.M. Du: J. Alloys Compd. 768 (2018) 316. DOI:10.1016/j.jallcom.2018.07.254
[15] E. Parthe, H. Nowotny, H. Schmid: Monatsh Chem Verw Teile Anderer Wiss. 86 (1955) 385. DOI:10.1007/BF00903622
[16] H. Nowotny, B. Lux, and H. Kudielka: Monatsh. Chem. 87 (1957) 447. DOI:10.1007/BF00902640
[17] J. Li, S.Y. Yang, Z. Shi, C.P. Wang, Y.W. Kang, X.J. Liu: J. Phase Equilib. Diffus. 38 (2017) 110. DOI:10.1007/s11669-017-0517-z
[18] M.E. Schlesinger, H. Okamoto, A.B. Gokhale, R. Abbaschian: 14 (1993) 502. DOI:10.1007/BF02671971
[19] J.F. Smith, O.N. Carlson, Alloy Phase Diagrams, ASM International, ASM Handbook, Russell (1992) 1196.
[20] Okamoto, H.J. Phase Equilib. Diffus. 2010, 31, 409–410. DOI:10.1007/s11669-010-9733-5

(Received February 10, 2019; accepted October 1, 2019; online since January 14, 2020)

Correspondence address

Dr. Chang-Rong Li, Professor
School of Materials Science and Engineering
University of Science and Technology Beijing
Beijing 100083
P. R. China
Tel.: +86 01082377789
E-mail: crli@mater.ustb.edu.cn

Bibliography
DOI 10.3139/146.111867
Int. J. Mater. Res. (formerly Z. Metallkd.)
111 (2020) 2; page 103–118

ISSN 1862-5282